PicoWatt infrared power measurement using an absolute cryogenic radiometer

S.M. Carr, S.I. Woods, T.M. Jung, A.C. Carter, and R.U. Datla

Optical Technology Division
National Institute of Standards and Technology (NIST)
100 Bureau Drive, Gaithersburg, MD 20899 USA

ABSTRACT

We report on initial measurements of the low-temperature thermal properties of a device that is similar to the experimental apparatus used for absolute cryogenic radiometry (ACR) within the Low Background InfraRed (LBIR) facility at NIST. The device consists of a receiver cavity mechanically and thermally connected to a temperature-controlled stage through a thin-walled polyimide tube which serves as a weak thermal link. In order to evaluate the functionality of the device for use in a cryogenic radiometer, we measured the thermal resistance and thermal time constant of the system within the temperature range of 1.8 - 4.4 K. The measured thermal resistance and thermal time constant at 1.883 K were 2400 ± 500 (K/mW) and 24 ± 6 (s). This value for the thermal resistance should result in about an order-of-magnitude improvement in radiometer sensitivity compared with the present ACR within LBIR. Although the sensitivity should improve by about an order-of-magnitude, the measured time constant is nearly unchanged with respect to previous ACRs within LBIR, due to the reduced dimensions of the receiver cavity. Finally, the thermal conductivity inferred from the measured thermal resistance and geometrical parameters was computed, with an average value of 0.015 (W/m-K), and compared with other measurements of polyimide from the literature.

Keywords: LBIR, NIST, absolute cryogenic radiometer, electrical substitution radiometer, IR, pW power

1. INTRODUCTION

The Low Background InfraRed (LBIR) facility[1,2] at the National Institute of Standards and Technology (NIST) is developing an advanced Absolute Cryogenic Radiometer (ACR) designed to enable the measurement and calibration of infrared power as low as 1 picoWatt (pW) with an accuracy on the order of 0.1%. For the advanced ACR, as with the present ACR infrared power standard at NIST,[3] radiant energy is converted into heat by the process of absorption and measured by electrical substitution methods. Absolute radiometry may be defined as "the use of electrically calibrated thermal detectors of optical radiation for the realization of an optical power scale".[4] The method of electrical substitution, which can be traced back to early work by Angstrom,[5] is used to measure the incident radiant power in absolute units. A solid-state trap detector will be calibrated by the advanced ACR and used to transfer the power scale.[6] The advanced detector pair will be used to establish and disseminate infrared power calibrations down to 1 pW with a combined uncertainty of about 0.1%.

The advanced ACR design is based on the ACRII model that is currently in use at the LBIR Facility.[3] Improvements in radiometer sensitivity are expected from: employing a more sensitive thermometer on the ACR receiver cavity, weakening the thermal link from the receiver cavity to the (second stage) heat sink, and operating at lower background temperature. The advanced ACR design includes reduced physical dimensions for the receiver cavity, in order to achieve a reasonable calculated thermal time constant given the potentially large reduction in the thermal conductance of the thermal link. In this paper we describe experimental results from an initial experimental configuration consisting of a receiver cavity with reduced dimensions and a thin-walled polyimide tube for the thermal link.

Further author information:
S.M.C.: E-mail: stephen.carr@nist.gov, Telephone: 301 975 3470

Infrared Technology and Applications XXXV, edited by Bjørn F. Andresen, Gabor F. Fulop, Paul R. Norton
Proc. of SPIE Vol. 7298, 72983Y · © 2009 SPIE · CCC code: 0277-786X/09/$18 · doi: 10.1117/12.820290

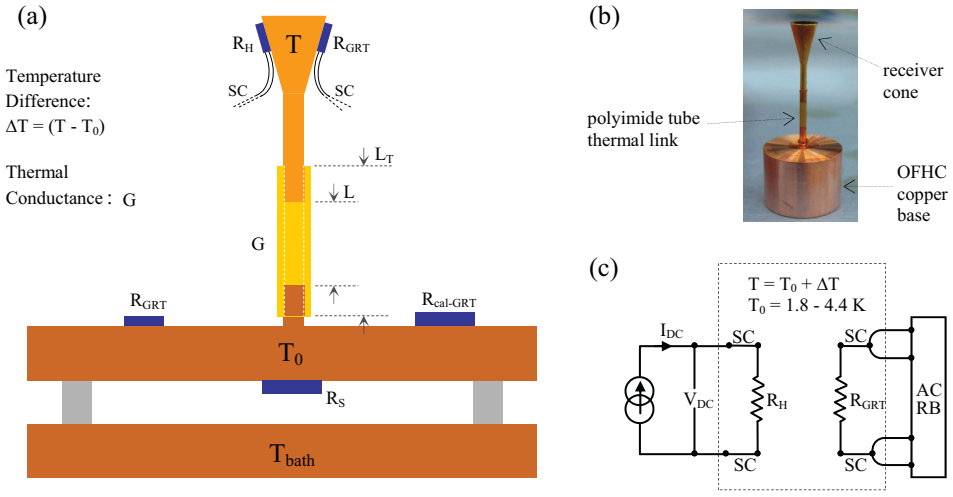

Figure 1. Experimental apparatus used for the measurements. (a) Schematic showing the components of the experimental platform. (b) Digital image of the device during the initial stages of assembly. (c) Schematic of the electrical measurement circuits.

2. EXPERIMENTAL DESCRIPTION

The experimental platform shown in Fig. 1(a) was enclosed in the evacuated sample space of a liquid helium cryostat. At low temperature the typical pressure in the sample space was less than or about 1.3 x 10^{-4} Pa (1.0 x 10^{-6} Torr). The bath temperature T_{bath} was reduced from about 4.2 K to about 1.8 K by pumping on the liquid helium. Partial thermal isolation between the OFHC copper sample stage at temperature T_0 and the bath at temperature T_{bath} was enabled through the use of four aluminum legs connecting the sample stage to the cryostat. A resistor heater R_s in combination with a germanium resistance thermometer R_{GRT} enabled control of the sample stage temperature T_0 using a standard PID algorithm. The sample stage temperature was monitored by the calibrated GRT labeled $R_{cal-GRT}$.

A receiver cavity, intended for use as a component of a cryogenic radiometer, was mechanically and thermally connected to the sample stage through the thermal link with thermal conductance G as shown in Fig. 1(a). A digital image of the actual apparatus during the initial stages of assembly is shown in Fig. 1(b). The receiver cavity, in the shape of a hollow cone, has a base diameter of 4 mm and is made from electroformed copper plated with gold. The thermal link was a polyimide tube with inner diameter 1.00 mm and wall thickness 38.1 μm (1.5 mils). Two different total tube lengths of L_T = 8.8 mm and L_T = 11.4 mm were used. The mechanical and thermal joints between the receiver cavity neck and the polyimide tube, as well as between the polyimide tube and the OFHC copper base, were made using GE varnish. Subtracting the overlap lengths of the joints from the total length L_T defines the conduction length L, as indicated in Fig.1 (a).

The temperature difference $\Delta T = (T - T_0)$ between the receiver cavity and the sample stage was induced and measured through a surface-mount resistor heater R_H and a bare-chip GRT resistance sensor R_{GRT} mechanically and thermally attached to the receiver cone using GE varnish. The electrical leads to R_H and R_{GRT} were 25.4 μm (1 mil) diameter copper-stabilized superconducting (SC) wire with a Nb-Ti superconducting core (T_c = 9 K) and copper sheath. The copper sheath was removed by etching except for short sections at the ends used for electrical contacts. The wires were threaded through polyimide tubes with 127 μm (5 mil) inner diameter and 19 μm (0.75 mil) wall thickness for mechanical strain relief and electrical insulation. A schematic of the electrical measurement circuits are shown in Fig. 1(c). A LakeShore * 370 AC Resistance Bridge (ACRB) was used for four-terminal resistance measurment of R_{GRT} on the receiver cone. After the stage temperature T_0 was

*Identification of particular manufacturers in this paper does not imply endorsement by the National Institute of Standards and Technology.

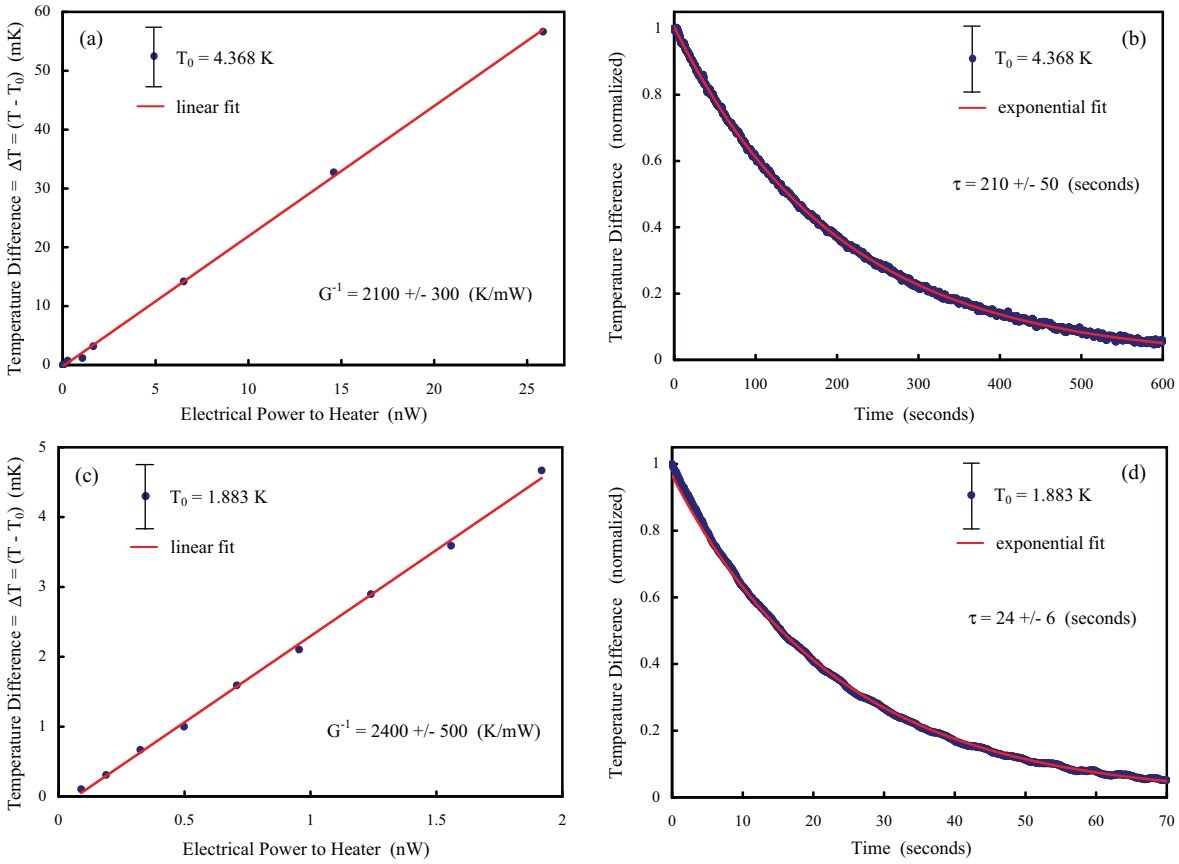

Figure 2. Measured temperature difference as a function of electrical power to heater and as a function of time after the electrical power to the heater was shut off. The top row ((a),(b)) is for $T_0 = 4.368$ K and the bottom row for $T_0 = 1.883$ K ((c),(d)). G^{-1} is defined as the slope from the least-squares linear fits. τ is the thermal time constant from the simple exponential fit, $a\, e^{(-t\,/\,\tau)}$.

stablized, a measurement of R_{GRT} established the resistance value corresponding to thermal equilibrium $T = T_0$. The temperature difference was computed from

$$\Delta T = \Delta R \,/\, (dR/dT) \tag{1}$$

where ΔR is the measured difference between the resistance at temperature T and the thermal equilibrium value corresponding to temperature T_0. The sensitivity (dR/dT) of R_{GRT} was measured over the relevant tempeature range in a previous experimental run. A low-noise DC current source, internal to the ACRB but a separate measurement circuit, was used as the heater output to drive DC current through the heater resistor R_H. The current I_{DC} and voltage V_{DC} were measured using an Agilent 3458A eight-digit multimeter. The DC electrical power delivered to the heater resistor is computed from $P = I_{DC} \cdot V_{DC}$. For the results presented here the heater output was operated in an open-loop mode with constant DC electrical power delivery without temperature feedback.

3. EXPERIMENTAL RESULTS

3.1 Thermal Resistance

We show in Fig. 2 the experimental data for two different stage temperatures, $T_0 = 4.368$ K ((a),(b)) and $T_0 = 1.883$ K ((c),(d)). We first focus on the two plots in the left column displaying the computed temperature difference as a function of the measured electrical power to the resistor heater. For these measurements the

objective was to obtain data starting with the lowest possible heater excitation powers that allowed a resolvable temperature difference. As shown in the figures, this resulted in a power range measured in nanoWatts. This can be compared with the power dissipated in the measurement of the resistor R_{GRT} on the receiver cavity, which was independently measured by the ACRB with a typical magnitude of 2 - 20 picoWatts. The data were fit using least-squares linear fits. The deviation of the data from linearity can be quantified through the coefficient of determination, which is 0.9994 for Fig. 1(a) and 0.9983 for Fig. 1(c), where a value of unity indicates no deviation from linearity. Assuming the thermal energy flux is proportional to the temperature gradient, and that the temperature gradient is constant, the thermal power is related to the temperature difference through

$$P = G \cdot \Delta T \tag{2}$$

where G is the thermal conductance of the system. Thus the slopes from the linear fits in Figs. 2(a) and 2(c) are the inverse of the thermal conductance, G^{-1}, also referred to as the thermal resistance, with the determined numerical values indicated on the plots. The uncertainty in the temperature difference is computed using Eq. (1) including the uncertainties from the measured resistance difference ΔR and measured sensitivity (dR/dT). The indicated uncertainty in the thermal resistance is the uncertainty in the slope resulting from the underlying uncertainty in the temperature difference. The relative uncertainty in the computed electrical heater power was as follows: 0.3% for $P \lesssim 0.1$ nW, 0.2% for 0.1 nW $\lesssim P \lesssim 0.5$ nW, and less than or about 0.1% for $P \gtrsim 0.5$ nW. Thus the error bars for the electrical power are negligibly small on the scale of the plots and are therefore not displayed. Other possible sources of uncertainty include the effects of thermal expansion, thermal contact resistance, radiative heat loss, thermal conductions through the SC Nb-Ti leads, and thermal conduction through the polyimide tubes containing the SC Nb-Ti leads.

3.2 Thermal Time Constant

Another observable of interest is the thermal time constant associated with the system. Starting from the largest temperature difference for a fixed T_0, the electrical power to the heater was turned off and the resulting rise[†] in resistance of the receiver cone sensor R_{GRT} was recorded through stabilization of the resistance at thermal equilibrium. The measured difference in resistance from thermal equilibrium can be converted to a temperature difference through Eq. (1). Figs. 2(b) and (d) show the temperature difference normalized by the initial value as a function of time for $T_0 = 4.368$ K and $T_0 = 1.883$ K. The data were fit using a simple exponential, $a\, e^{(-t\,/\,\tau)}$, where τ is the thermal time constant indicated on the plots. The deviation of the simple exponential fits from the data can be be quantified through the coefficient of determination, which is 0.9985 for Fig. 1(b) and 0.9988 for Fig. 1(d), where a value of unity indicates no deviation. The uncertainty in the normalized temperature difference is computed from the uncertainties in the resistance measurements. The indicated uncertainty in the thermal time constant is the uncertainty in the simple exponential fit resulting from the underlying uncertainty in the normalized temperature difference.

Table 1 lists the experimental results for the investigated range of polyimide tube lengths and temperatures. The symbol k is the thermal conductivity (W/m-K) inferred from the measured thermal resistance and geometrical parameters, which will be discussed in the next section. There are several aspects of the data to be discussed. Focusing first on the L = 4.7 mm data, it is apparent that the measured thermal resistance has a rather weak temperature dependence over the investigated temperature range. The thermal time constant, however, is reduced by nearly an order of magnitude in lowering the temperature from $T_0 = 4.368$ K to $T_0 = 1.883$ K. This may be understood by writing the thermal time constant as the product, $\tau = G^{-1} \cdot C$, where G^{-1} is the thermal resistance and C is the total heat capacity of the system. Then the ratio $[(\tau/G^{-1})_{4.4K} \,/\, (\tau/G^{-1})_{1.9K}] \approx 10 \approx (C_{4.4K}/C_{1.9K})$, the ratio of the total heat capacities. Assuming the Debye T^3 law is obeyed, the ratio of the heat capacities is $(C_{4.4K}/C_{1.9K}) = (4.4/1.9)^3 \approx 12$, in agreement with the measured ratio within the uncertainties of the measurements. The thermal resistance, and therefore the inferred thermal conductivity, is typically observed to have a much weaker temperature dependence than the heat capacity in this temperature range, similar to the measured values for this system presented in Table 1.

Finally, before proceeding to the next section, we briefly discuss the bottom row of Table 1, which displays the results for a longer L = 7.7 mm polyimide tube. The shorter polyimide tube was removed and replaced

[†]GRTs are negative-temperature-coefficient devices at low temperature: $(dR/dT) < 0$.

Table 1. System parameters and measured values for this work. k is the thermal conductivity inferred from the measured thermal resistance and geometrical parameters. The thermal time constant for L = 7.7 mm was not measured.

L_T (mm)	L (mm)	T_0 (K)	G^{-1} (K/mW)	k (W/m-K)	τ (s)
8.8	4.7	4.368	2100	0.018	210
8.8	4.7	4.234	2300	0.016	170
8.8	4.7	4.001	2500	0.015	130
8.8	4.7	3.799	2400	0.016	160
8.8	4.7	1.883	2400	0.016	24
11.4	7.7	4.368	5200	0.012	-

with the longer tube, with care taken to minimize the disturbance to the system. The thermal resistance of the longer tube was measured at $T_0 = 4.368$ K to allow comparison with the shorter tube which was also measured at $T_0 = 4.368$ K. Assuming the thermal resistance is proportional to the length of the polyimide tube, the ratio $[(G^{-1})_{7.7\mathrm{mm}}/(G^{-1})_{4.7\mathrm{mm}}]$ should be equal to $(L_{7.7\mathrm{mm}}/L_{4.7\mathrm{mm}})$. This equality holds when considering the worst-case uncertainties. From this measurement we conclude that the thermal resistance of the polyimide tube is the dominant thermal resistance in the system. There is, however, at least one additional source of uncertainty, which is the different thermal contact resistances for the shorter and longer tubes; consistency in the thermal contact resistance is difficult to control experimentally.

3.3 Thermal Conductivity

From the measured thermal resistances and geometrical parameters it is possible to compute the thermal conductivity from

$$k = \mathrm{G}\left(\frac{\mathrm{L}}{\mathrm{A}}\right) \tag{3}$$

where $\mathrm{A} = \pi\,(r_2^2 - r_1^2)$ is the cross-sectional area with r_1 and r_2 the inner and outer radii of the polyimide tube . The values computed from Eq. (3) are listed in Table 1 and shown with their uncertainties in Fig. 3. As thermal conductivity is a material property, computation of the thermal conductivity from the measured data allows comparison with other measurements from the literature. In Fig. 3 we include the results from seven independent measurements of the thermal conductivity of polyimide. The power law fits shown in Fig. 3 are detailed in Table 2 along with the reference, the polyimide type, the temperature range of the measurements, and the estimated maximum error in the power law fits.

Lawrence et al. discussed the fact that the results presented in the literature give inconsistent values for the thermal conductivity of various types of polyimide at 4.2 K. The works of Radebaugh et al. and Wipf suggest that the thermal conductivity should be between 0.004 and 0.005 (W/m-K); whereas Rule et al. and an extrapolation of the work of Yokoyama suggest the value should be between 0.010 and 0.015 (W/m-K). In the work of Lawrence et al. the thermal conductivity of Kapton HN was measured between 0.5 and 5 K. They concluded that their measurements were consistent with the works of Rule et al., Wipf , and Yokoyama and that their measurements were inconsistent with those of Radebaugh et al.

In Fig. 3, along with the results from this work, we have added two additional curves for comparison that were not considered in Lawrence et al. These are the thermal conductivity curve fit from the NIST Cryogenic Technologies Group Material Properties Index and the work of Zhang et al. Considering the results from this work around 4.2 K, the total range of values for the thermal conductivity including uncertainty is 0.008 to 0.022 (W/m-K) with an average value of 0.015 (W/m-K). Around 4.2 K, our values for the thermal conductivity are consistent with those of Lawrence et al., Rule et al., the NIST Cryo. Tech. curve fit, and extrapolation of the work of Yokoyama. Our results appear to be inconsistent with those of Zhang et al. and are definitely inconsistent with those of Radebaugh et al. Note that the polyimide type for Radebaugh et al. was unspecified and that the polyimide type for Zhang et al. was Vespel SP-1. As discussed in Lawrence et al. , there may be large differences in the low-temperature thermal conductivity of different types of Kapton.

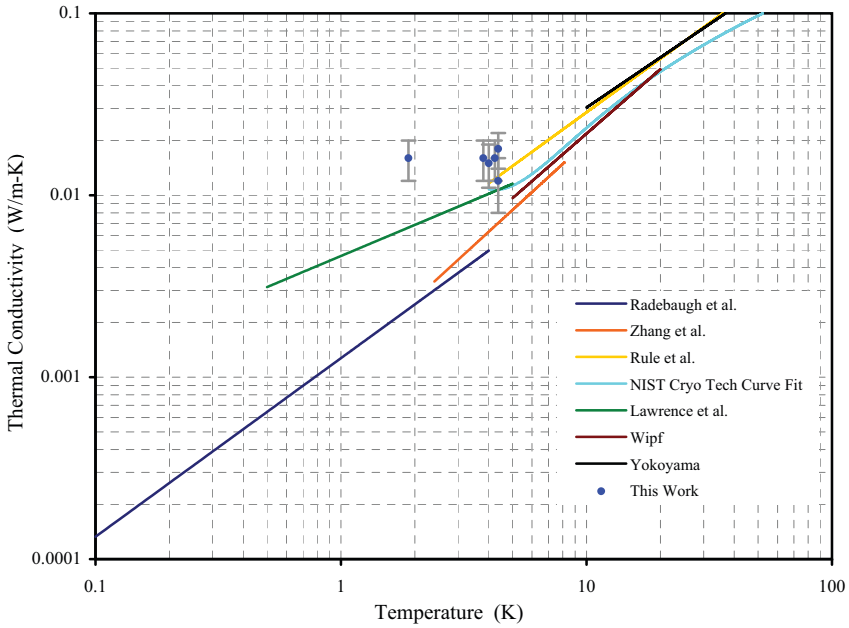

Figure 3. Thermal conductivity of polyimide as a function of temperature for this work and for other results from the literature. The lines are the literature results from the power law fits in Table 2.

Table 2. Comparison of the measured thermal conductivity from this work with other results from the literature.

Reference	Polyimide Type	Temperature Range (K)	Power Law Fit k in (W/m-K) T in (K)	Estimated Maximum Error in Fit
Radebaugh et al.[7]	Unspecified	0.02 - 4	$k = 1.273 \times 10^{-3} \cdot T^{0.9817}$	3%
Zhang et al.[8]	Vespel SP-1	2.4 - 8.0	$k = 1.137 \times 10^{-3} \cdot T^{1.2358}$	1%
Rule et al.[9]	Kapton HN	4 - 300	$k = 2.996 \times 10^{-3} \cdot T^{0.9794}$	2%
NIST Cryo. Tech. Group[10]	Kapton HN	4 - 300	Eighth-Order Log Expansion	2%
Lawrence et al.[11]	Kapton HN	0.5 - 5	$k = 4.638 \times 10^{-3} \cdot T^{0.5678}$	20%
Wipf[12]	Unspecified	5 - 20	$k = 1.451 \times 10^{-3} \cdot T^{1.177}$	2%
Yokoyama[13]	Kapton H	10 - 300	$k = 3.687 \times 10^{-3} \cdot T^{0.9154}$	5%
This Work[14]	Ref. [14]	1.8 - 4.4	N/A	N/A

The thermal conductivity data point from this work for $T_0 = 1.883$ K appears to imply a temperature dependence that is flat or very weak over the investigated temperature range. However, the absence of data in the approximate range of 2 - 4 K does not allow a meaningful temperature dependence to be extracted. For the $T_0 = 1.883$ K data point from this work in Fig. 3, the inferred value of the thermal conductivity is 0.016 (W/m-K). This is more than a factor of two larger than the value from the power law fit of Lawrence et al. at the same temperature. As noted above, for the data from this work around 4.2 K, the average value for the thermal conductivity is 0.015 (W/m-K). This average value around 4.2 K is approximately 50% larger than the power law fit values for Lawrence et al. and the NIST Cryo. Tech. Curve Fit and approximately 25% larger than the power law fit value for Rule et al. These observations motivate the consideration of possible systematic effects that could result in measured values for the thermal conductivity that are larger than the actual values. Parallel thermal conduction, through the SC Nb-Ti leads or through the polyimide tubes containing the SC Nb-Ti leads, would result in a measured effective thermal resistance that is lower than the thermal resistance for the polyimide

tube alone, meaning the actual thermal resistance would be higher than the measured value. This would result in a lower inferred thermal conductivity. Another possible systematic effect could result from power loss. If the actual thermal power through the polyimide tube was lower than the measured electrical power, for example due to radiative heat loss, this would also result in an actual thermal resistance that is greater than the measured value, also resulting in a lower inferred thermal conductivity. Finally, it is possible that the chemical composition for this particular polyimide type and/or the particular process used to fabricate the polyimide tube result in a thermal conductivity which is indeed larger than other types of polyimide.

4. CONCLUSION

We have described our initial measurements of the low-temperature thermal properties of a device that is similar to the experimental apparatus used for absolute cryogenic radiometry within the Low Background InfraRed (LBIR) facility at NIST. For the ACRII[3] presently in use within LBIR, the central element of the experimental configuration is a receiver cone that is mechanically and thermally connected to a temperature-controlled stage through a weak thermal link; the larger the thermal resistance of the thermal link the greater the sensitivity of the radiometer. The device investigated in this work utilized a thin-walled polyimide tube for the thermal link. In order to evaluate the functionality of the device for use in a cryogenic radiometer, in particular the low-temperature thermal properties of the thermal link, in this work we measured the thermal resistance and thermal time constant of the system. The thermal conductivity inferred from the measured thermal resistance and geometrical parameters was computed and compared with other measurements of polyimide from the literature.

The inferred values of the thermal conductivity are in the range of 0.012 - 0.018 (W/m-K), with an average value of 0.015 (W/m-K), within the investigated temperature range of 1.8 - 4.4 K. The inferred values around 4.2 K are consistent within the uncertainty of the measurements with most of the other values from the literature, where a typical value is approximately 0.011 (W/m-K). For the shorter polyimide tube used in this work the measured thermal resistance values were in the range of 2100 - 2500 (K/mW). This range is approximately an order-of-magnitude larger than the thermal resistance for the ACRII, which should result in an order-of-magnitude improvement in the sensitivity of a next-generation ACR using a similar polyimide tube for the thermal link. For the receiver cone with a base diameter of 4 mm used in this work, the measured thermal time constant at 1.883 K was 24 $\pm$ 6 (s), which is close to both the ACR value of 22 (s) and the ACRII value of 17 (s).[3] Thus the sensitivity of the next-generation ACR should increase by approximately an order-of-magnitude while the time constant should be nearly unchanged compared with the ACR and ACRII radiometers. A refined experimental configuration, including a polyimide tube with similar length but reduced wall thickness, has been assembled. Initial measurements using the refined configuration reveal the expected increase in thermal resistance and consistency with the results presented in this work.

REFERENCES

[1] Carter, A.C., Datla, R.U., Woods S.I., and Jung T.M., "Infrared absolute calibrations down to 10 fW in low-temperature environments at NIST," Proc. SPIE 7021, 70210S (2008).

[2] Carter, A. C., Datla, R. U., Jung, T. M., Smith, A. W. Fedchak, J. A., "Low-background temperature calibration of infrared blackbodies," Metrologia, 43, S46-S50 (2006).

[3] Carter A.C., Lorentz S.R., Jung T.M., Datla R.U., "ACR II: Improved absolute cryogenic radiometer for low background infrared calibrations,"' Applied Optics 44, 871-875 (2005).

[4] Hengstberger F., [Absolute Radiometry], Academic Press Inc., San Diego, CA, (1989).

[5] Angstrom K., "The Quantitative Determination of Radiant Heat By the Method of Electrical Compensation," Transactions of the Royal Society of Sciences, Upsala (1893).

[6] Carter, A. C., Woods S.I., Carr S.M., Jung T.M., Datla R.U., "Absolute cryogenic radiometer and solid state trap detectors for IR power scales down to 1 pW with 0.1% uncertainty," to appear in Metrologia (2009).

[7] Radebaugh R., Frederick N.V., Siegwarth J.D., "Flexible laminates for thermally grounded terminal strips and shielded electrical leads at low temperature,"' Cryogenics 13, 41-43, (1973).

[8] Zhang, Z.M., Lorentz, S.R., Rice, J.P., Datla, R.U., "Measurement of thermophysical properties of polyimide and a black paint for future development of cryogenic radiometers," Metrologia 35, 511-515 (1998).

[9] Rule, D.L., Smith, D.R., Sparks, L.L., "Thermal conductivity of a polymide film between 4.2 and 300 K, with and without alumina particles as filler," NISTIR 3948, (1990).

[10] Materials Properties section of the NIST Cryogenic Technologies Group website: http://cryogenics.nist.gov/.

[11] Lawrence J., Patel A.B., Brisson, J.G., "The thermal conductivity of Kapton HN between 0.5 and 5 K," Cryogenics, 40, 203-207 (2000).

[12] Wipf, S.L., "Low temperature heat transfer by contact in vacuo, and thermal conductivity of Kapton," Proceedings of the Ninth International Conference on Magnet Technology, Villiigen. Marinucci C., Weymuth P., editors. Swiss Inst Nucl Res., 692-695 (1985).

[13] Yokoyama H., "Thermal conductivity of polymide film at cryogenic temperature," Cryogenics 35, 798-799, (1995).

[14] The polyimide tubing used for the thermal link was manufactured by RiverTech Medical, LLC. The base material is Pyre-M.L. RC5019 Wire Enamel, which is 15-16% Polyamic Acid of Pyromellitic Dianhydride/4,4-Oxydianiline, from Industrial Summit Technology Corporation (www.istusa.com). Identification of particular manufacturers in this paper does not imply endorsement by the National Institute of Standards and Technology.